Dirac nodal lines and large spin Hall effect in the 6H-perovskite iridate Ba_{3}TiIr_{2}O_{9}

Sayantika Bhowal and S. Satpathy

Phys. Rev. B **100**, 115101 — Published 3 September 2019

DOI: 10.1103/PhysRevB.100.115101

Dirac Nodal Lines and Large Spin Hall Effect in the 6H Perovskite Iridate $Ba_3TiIr_2O_9$

Sayantika Bhowal* and S. Satpathy
Department of Physics & Astronomy, University of Missouri, Columbia, MO 65211, USA

Nodal line semi-metals with symmetry protected band structure offer a platform for the investigation of a number of emerging quantum phenomena. Using first-principles calculation combined with symmetry analysis, we show that $Ba_3TiIr_2O_9$ hosts Dirac nodal line (DNL) along the A-L direction of the Brillouin zone, protected by the glide reflection symmetry. In the presence of the spin-orbit coupling, even though the DNL along A-L direction is protected, DNLs along other directions as well as multiple nodal loops present in the system gap out. The gapped out Dirac nodal loops act as a source of spin Berry curvature, resulting in a large spin Hall conductivity ($\approx 300\ \frac{\hbar}{e}\ \Omega^{-1}\text{cm}^{-1}$). This suggests the possible application of the material as a spin current detector.

Topological semi-metals (TSM) are characterized by the non-accidental band-crossings which can not be removed by the perturbation of the Hamiltonian without breaking any of its symmetry. The search for new materials hosting gapless topological states has been an active area of research over the past decade [1–3], driven in part by the prediction of a plethora of exotic quantum phenomena for these systems such as the chiral anomaly [4], topological transport [5], and quasi-topological electromagnetic response [6].

The two typical examples of 3D TSM, viz., Dirac and Weyl semi-metals have respectively four-fold and two-fold degenerate band-crossings near the Fermi level, the low energy excitations of which are respectively Dirac and Weyl fermions, well known in the standard model of relativistic high-energy physics. In contrast to the zero dimensional band-crossings in Dirac and Weyl semi-metals, nodal line semi-metals have bands that cross each other along a line [7] and have low energy excitations which do not have any high-energy counterpart. Such nodal lines are protected by the non-symmorphic symmetry which, in turn, is predicted to give rise to intriguing nodal-fermion features that include hourglass fermions [8], Möbius-twist surface states [9] and nodal chains [10]. These various fascinating predictions result in a growing field of research based on the material realization of the nodal line semi-metals [11, 12]. The presence of the nodal lines may also suggest the possibility of a large spin Hall effect (SHE) [13], a phenomenon where the electric current is converted into a spin current and hence is at the heart of the spintronics. A variety of exotic phases including the quantum spin liquid state has already been reported [14] for a number of iridates belonging to the 6H family, the subject of the present work.

In the present work, we have predicted the presence of Dirac nodal line, which is protected by the non-symmorphic glide reflection symmetry, in the 6H perovskite iridate $Ba_3TiIr_2O_9$ (BTIO), a material that has been synthesized previously [15]. The material hosts multiple Dirac nodal lines and loops (DNL) in the mirror planes in the absence of spin-orbit coupling (SOC), which become gapped out with the inclusion of the SOC except along the A $\rightarrow$ L direction of the hexagonal Brillouin zone (BZ), enforced by the off-centered glide reflection. Not surprisingly, owing to the small energy denominator in the Kubo expression, the gapped out nodal loops facilitate a large spin Berry curvature $\Omega^{\eta}_{n,\mu\nu}(\vec{k})$, the central quantity in the determination of the SHE [13]. Explicit calculations presented below show that BTIO exhibits a large spin Hall conductivity (SHC), and therefore may have potential application in spintronics as a spin current detector. In addition, we find that the DNLs can be transformed into Weyl nodal lines (WNL) by the application of an external magnetic field.

BTIO crystallizes in the hexagonal centro-symmetric $P6_3/mmc$ space group in the 6H perovskite structure (stacking sequence hcchcc) [15] containing face-shared IrO_6 octahedra, arranged on a triangular network (Fig. 1). The structure hosts 24 symmetry operations that include three equivalent mirror-reflection planes $\mathcal{M}_{100}$, $\mathcal{M}_{010}$, $\mathcal{M}_{110}$ as well as the off-centered glide reflection (reflection plus translation) $\tilde{\mathcal{M}}_z \equiv \{\mathcal{M}_z|\vec{\tau} = \frac{\hat{z}}{2}\}$. Magnetic measurements [15] show that the system does not exhibit any long range magnetic order down to 1.8 K, consistent with the recent density functional calculations, which found a non-magnetic ground state below a critical value of U ($U_c \approx 3.5$ eV) [16]. Thus in addition to the inversion ($\mathcal{I}$) and non-symmorphic ($\tilde{\mathcal{M}}_z$) symmetry, we also have the time-reversal (TR) symmetry ($\mathcal{T}$), all essential ingredients to protect the DNL in any material.

Band calculations were performed using the density functional theory (DFT) with the plane wave basis and the generalized-gradient approximation [17], as implemented in the VASP code [18]. In the absence of SOC, multiple DNLs in the band structure are formed in the $k_z = \pi$ plane of the BZ in addition to the Dirac nodal loops in the three planes ($k_x = 0$, $k_y = 0$, and $k_z = 0$) as indicated schematically in Fig. 2. All bands along the DNLs are four-fold degenerate. The existence of the Dirac nodal loops may be inferred by examining the band structure shown in Fig. 2 (c) for symmetry lines in the $k_z = 0$ plane in the BZ. The band crossing along M$\rightarrow\Gamma$ involves states with B_1 and B_2 symmetries of the little group C_{2v} with opposite mirror eigenvalues. This band crossing persists along all directions in the $k_z = 0$ plane,

* bhowals@missouri.edu

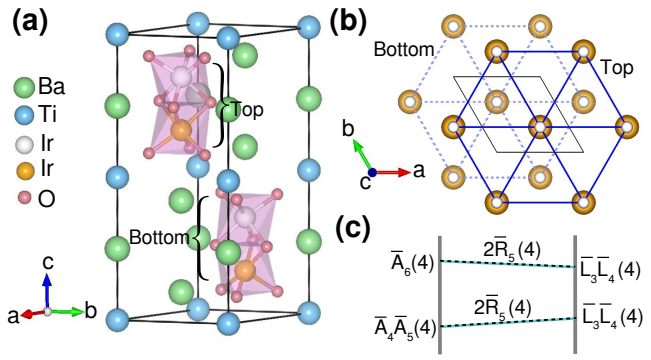

FIG. 1. (a) The hexagonal unit cell of BTIO, consisting of two formula units $(Ba_3TiIr_2O_9)_2$ with each Ir atom in an octahedral environment. Two face-sharing IrO_6 octahedra form an Ir dimer (the two Ir atoms of the dimer are colored white and orange). (b) The triangular network formed by the dimers as viewed from the top. As a result of the inversion $\mathcal{I}$ and the off-centered glide reflection $\tilde{\mathcal{M}}_z$, the centre of the triangular network formed by the top dimer is shifted with respect to the same for the bottom dimer (connected by the dashed line). (c) The band connectivity for the space group $P6_3/mmc$ along the the $A-R-L$ line, which forms the four-fold degenerate DNL, protected by symmetry.

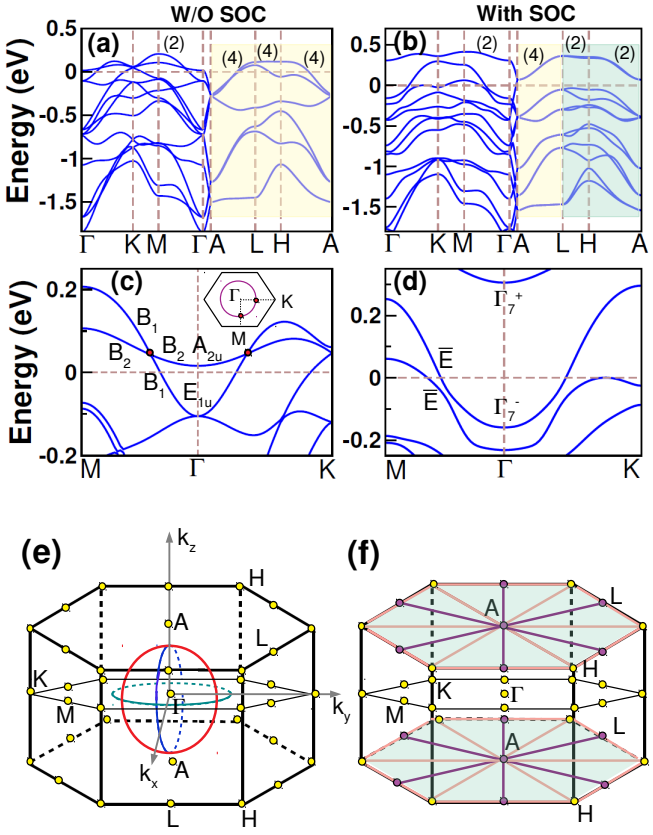

FIG. 2. Density-functional band structure of BTIO, both in the absence (a, c) and presence (b, d) of the SOC, indicating the presence of DNLs in both cases. Figs. (e) and (f) show the DNLs in the absence of SOC, of which only the star-like DNL (purple lines in (f)) along $A \to L$ is symmetry-protected in the presence of SOC. Fig. (c) indicates the presence of a Dirac nodal loop in the band structure (*inset* shows the full loop), while the gapping out of the loop in the presence of the SOC is apparent from Fig. (d). The unshaded (shaded) regions in (a) and (b) correspond to the $k_z = 0$ ($k_z = \pi$) plane of the BZ.

resulting in a nodal loop. Similar nodal loops exist on the $k_x = 0$ and $k_y = 0$ planes as well.

In the presence of SOC, the four-fold degenerate DNLs gap out, resulting in two 2-fold degenerate states at each k point, except that the DNL along A $(0,0,\pi) \to$ L $(\pi,0,\pi)$ in the $k_z = \pi$ plane is still protected by the glide reflection $\tilde{\mathcal{M}}_z$, leading to a star-like structure, resulting from the six-fold rotational symmetry of the crystal structure, as shown in Fig. 2 (f). This gapping out along a large number of k points plays a central role in producing the large SHC as discussed later.

Glide reflection and Dirac nodal lines: The glide reflection symmetry is an essential ingredient for the formation of the DNLs with four fold degeneracy. To show this, we imagine that we have found a solution $|\Psi\rangle$ with energy ε at a Brillouin zone point k, for which $\mathcal{I}$, $\mathcal{T}$, and glide reflection $\tilde{\mathcal{M}}_z$ are symmetry elements of the little group of k which is true for the k points A and L on the $k_z = \pi$ plane and Γ and M on the $k_z = 0$ plane. These k points in the BZ are the so-called TR invariant momentum (TRIM) points, because under TR, they are transformed back to themselves due to the fact that the time-reversed momentum is connected via a reciprocal lattice vector ($-\vec{k} = \vec{k} + \vec{G}$). We will see that we can generate four orthogonal states with the same energy for points along $A \to L$, resulting in the DNL, with the four-fold degeneracy protected by the glide reflection $\tilde{\mathcal{M}}_z$, but not along $\Gamma \to M$.

Consider first the $k_z = 0$ and $k_z = \pi$ planes, for which the glide reflection is a symmetry element and $[H_k, \tilde{\mathcal{M}}_z] = 0$, so that we can construct simultaneous eigenstates of H_k and the glide reflection $\tilde{\mathcal{M}}_z : (x,y,z) \to (x,y,-z+\frac{1}{2})i\sigma_z$. Since $\tilde{\mathcal{M}}_z^2 = -\mathbb{I}$, all Bloch states within these planes can be chosen to have definite $\tilde{\mathcal{M}}_z$ eigenvalues, i.e., $\tilde{\mathcal{M}}_z |\Psi_\pm\rangle = \pm i |\Psi_\pm\rangle$, with the correponding energy ε_+ or ε_-. We can then construct four eigenstates with the same energy for each case as indicated in Table I.

Table I is obtained by the successive application of the symmetry operations $\tilde{\mathcal{M}}_z$ and $\mathcal{I} : (x,y,z) \to (-x,-y,-z)$, from which we can see that

$$\tilde{\mathcal{M}}_z \mathcal{I} |\Psi_\pm(\vec{k})\rangle = e^{2\pi i(\vec{k}\cdot\vec{\tau})} \mathcal{I} \tilde{\mathcal{M}}_z |\Psi_\pm(\vec{k})\rangle . \qquad (1)$$

This shows that $\mathcal{I}|\Psi_\pm\rangle$ is also an eigenstate of $\tilde{\mathcal{M}}_z$ with similar and opposite glide symmetry eigenvalues for the $k_z = 0$ and π planes respectively. Similarly, for the TR symmetry, $\mathcal{T} = i\sigma_y\kappa$ (κ is the complex conjugation operator), we have the result $\tilde{\mathcal{M}}_z \mathcal{T} |\Psi_\pm(\vec{k})\rangle =$

TABLE I. The two sets of four eigenstates each, one set generated from $\Psi_+(\vec{k})$ and the other from $\Psi_-(\vec{k})$, for $\vec{k}$ on the $k_z = 0$ or the $k_z = \pi$ plane. As discussed in the text, the $\tilde{\mathcal{M}}_z$ eigenvalues indicate symmetry-protected four-fold degenerate states at the TRIM points A and L on the $k_z = \pi$ plane, but not at the TRIM points Γ and M located on the $k_z = 0$ plane.

Index	Eigenstates of $\tilde{\mathcal{M}}_z$	Eigenvalues of $\tilde{\mathcal{M}}_z$ $k_z = 0$	$k_z = \pi$
(i)	$\|\Psi_\pm\rangle$	$\pm i$	$\pm i$
(ii)	$\mathcal{I}\|\Psi_\pm\rangle$	$\pm i$	$\mp i$
(iii)	$\mathcal{T}\|\Psi_\pm\rangle$	$\mp i$	$\mp i$
(iv)	$\mathcal{IT}\|\Psi_\pm\rangle$	$\mp i$	$\pm i$

$-\mathcal{T}\tilde{\mathcal{M}}_z|\Psi_\pm(\vec{k})\rangle$, which yields the glide symmetry eigenvalues for the time reversed state.

Using Table I, it is now easy to show that the energy bands at the TRIM points A and L are four-fold degenerate protected by symmetry, while no such protection exists for the TRIM points Γ and M. The TRIM points have the additional inversion and TR symmetry, because as stated above $-\vec{k} = \vec{k}+\vec{G}$, so that now we have $[H_k, S] = 0$, where $S = \mathcal{I}$, $\mathcal{T}$, or $\tilde{\mathcal{M}}_z$. This means that the two sets of four eigenstates have the same energy, ε_+ for the Ψ_+ set and ε_- for the Ψ_- set. All that remains to be shown now is that the four individual wave functions within the set don't interact among themselves, so that the four-fold degeneracy is preserved. The TR symmetry demands the double degeneracy for the Kramer's doublets, $(\Psi, \mathcal{IT}\Psi)$ and $(\mathcal{I}\Psi, \mathcal{T}\Psi)$. At the TRIM points on the $k_z = \pi$ plane, they can't hybridize since these two doublets have opposite $\tilde{\mathcal{M}}_z$ eigenvalues, leading to the four-fold degeneracy. At the Γ and M TRIM points on the $k_z = 0$ plane, however, there is no such symmetry protection from $\tilde{\mathcal{M}}_z$, and the two Kramer's doublets can hybridize, so that the four-fold degeneracy is not guaranteed. This is seen from the band structure presented in Fig. 2 (b), and it is consistent with the dimensions of the irreducible representations (IR) as indicated in Fig. 1 (c). A similar argument leads to the four-fold degeneracy along the $A \to L$ line (R point), and it also follows from the connectivity of the IRs.

Connectivity of the Bloch bands along $A \to L$ line: The occurrence of the DNL along A $\to$ L can be argued from the connectivity of the Bloch bands, determined from the corresponding double valued IRs in presence of TR symmetry. The double valued IRs at the TRIM point A are $\bar{A}_4$, $\bar{A}_5$ and $\bar{A}_6$, out of which $\bar{A}_4$ and $\bar{A}_5$ are two-dimensional complex IRs, while $\bar{A}_6$ is four-dimensional pseudo real IR. Now, pseudo-real IRs are TR symmetric by themselves while complex IRs are needed to be paired up to construct the TR symmetric IRs [19]. Thus the TR symmetric IRs at the A point are $\bar{A}_6$ (4) and $\bar{A}_4\bar{A}_5$ (4). Similarly, the TR symmetric IR at the L point is $\bar{L}_3\bar{L}_4$ (4) constructed from the two-dimensional complex double valued IRs $\bar{L}_3$ and $\bar{L}_4$. The TR symmetric IR at the intermediate point R $(u, 0, \frac{1}{2})$ is $2\bar{R}_5(4)$ constructed from two-dimensional and real double valued IR $\bar{R}_5$. All Bloch bands along the A $\to$ R $\to$ L, satisfying the compatibility relations $\bar{A}_6(4) \to 2\bar{R}_5(4)$ and $\bar{A}_4\bar{A}_5(4) \to 2\bar{R}_5(4)$ will, therefore, lead to four-fold degenerate DNL, as seen from Fig. 1 (c).

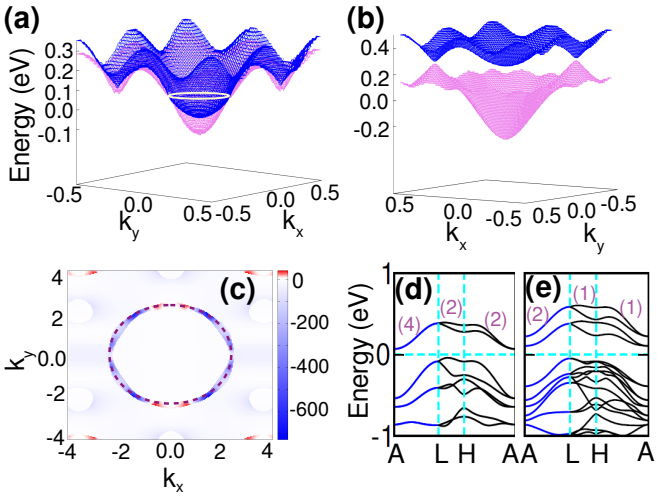

FIG. 3. DNLs and Spin Berry curvatures obtained from the model calculation, Eqs. (2) and (4). (a) The Dirac nodal loop in the absence of SOC (similar loops exist in the $k_y - k_z$ and $k_x - k_z$ planes as indicated in Fig. 2 (e). (b) The gapping out of the same nodal loop in the presence of SOC ($\lambda = 0.4$ eV). (c) Spin Berry curvatures $\Omega^x_{zy}(\vec{k})$ (units of Å^2) in the same plane, showing the dominant contributions from the gapped-out nodal loop. Figs. (d) (B = 0) and (e) (B = 0.5 eV) show the transformation of the DNLs along $A \to L$ into pairs of WNLs under the application of an external magnetic field.

The DNLs are captured within a Ir-d tight-binding (TB) model for the hexagonal lattice of BTIO, but keeping only the four Ir atoms in the unit cell. The Hamiltonian is

$$\mathcal{H} = \sum_{il\sigma,jm\sigma} t^{lm}_{ij} c^\dagger_{il\sigma} c_{jm\sigma} + \frac{\lambda}{2} \sum_\eta \sum_{il\sigma,m\sigma'} c^\dagger_{il\sigma} L^\eta_{lm} \sigma^\eta_{\sigma\sigma'} c_{im\sigma'}, \tag{2}$$

where $il\sigma$ are the site, orbital, and spin indices, η denotes the three cartesian components, λ is the SOC, $\vec{L}$ is the orbital angular momentum, $\vec{\sigma}$ is the electron spin, and the Hamiltonian parameters including the hopping t^{lm}_{ij} are extracted from the DFT results [20]. The computed eigenvalues of the Hamiltonian (2) reproduce the DNLs for both with and without SOC, consistent with the DFT results, as it must, since it is a property of the symmetry.

The SHC $\sigma^\eta_{\mu\nu}$ is computed from the momentum sum of the spin Berry curvatures $\Omega(\vec{k})$

$$\sigma^\eta_{\mu\nu} = \frac{e}{N_k V_c} \sum_{n\vec{k}}^{occ} \Omega^\eta_{n,\mu\nu}(\vec{k}), \tag{3}$$

where η, μ, ν are cartesian components, $j^{s,\eta}_\mu = \sigma^\eta_{\mu\nu} E_\nu$ is the spin current density along the μ direction with the

TABLE II. Spin Hall conductivity for BTIO, computed using the Kubo formula Eq. (3).

Components	SHC ($\frac{\hbar}{e}$ Ω^{-1}cm^{-1})
σ^z_{xy}	-12
σ^x_{yz}	47
σ^x_{zy}	-302

spin polarization along η, generated by the electric field along the ν direction, n is the band index, and V_c and N_k are respectively the primitive cell volume and the number of k points used in the BZ sum. Analogous to the ordinary Berry curvature, the spin Berry curvature is evaluated from the Kubo formula

$$\Omega^{\eta}_{n,\mu\nu}(\vec{k}) = -2\hbar^2 \sum_{n' \neq n} \frac{\mathrm{Im}[\langle\psi_{n\vec{k}}|\mathcal{J}^{\eta}_{\mu}|\psi_{n'\vec{k}}\rangle\langle\psi_{n'\vec{k}}|v_{\nu}|\psi_{n\vec{k}}\rangle]}{(\varepsilon_{n'\vec{k}} - \varepsilon_{n\vec{k}})^2}, \tag{4}$$

where the spin current operator is $\mathcal{J}^{\eta}_{\mu} = \frac{1}{4}\{v_{\mu}, \sigma_{\eta}\}$, with $v_{\mu} = \frac{1}{\hbar}\frac{\partial H}{\partial k_{\mu}}$ being the velocity operator. It can be easily seen from the Kubo formula that with both inversion and TR symmetries present, as is the case here, the spin Berry curvature is non-zero, while the ordinary Berry curvature would vanish in this case.

The SOC mixes the different spin components of the wave functions making the numerator in (4) non-zero, so that those DNLs that gap out (due to the same SOC) make a large contribution to the SHC due to the small energy denominator. This is seen from the numerical results [Fig. 3 (c)], where the spin Berry curvature sum $\sum_n^{occ} \Omega^x_{zy}(\vec{k})$ shown for the $k_z = 0$ plane has a strong contribution coming from the gapped-out Dirac nodal loop which exists on this plane. Since a large number of the DNLs gap out due to the SOC as indicated from Fig. 2, their contributions add up resulting in a large SHC for BTIO ($\approx 45\%$ of the total SHC). The contributions from the DNL and the rest of the Brillouin zone are discussed in detail in the Supplemental Materials [21].

We note that even though the DNLs along L-H and A-H also gap out (see Fig. 2), the corresponding contributions to $\sum_n^{occ} \Omega^x_{zy}(\vec{k})$ are relatively less due to the fact that the gapped-out bands, having opposite signs of spin Berry curvatures, are either both occupied or both unoccupied, leading to a net small contribution (~ 10 Å^2) as compared to the gapped-out Dirac nodal loops (~ 300 Å^2).

The crystal symmetry of BTIO allows just three independent elements [23], viz., $\sigma^z_{xy} = -\sigma^z_{yx}$, $\sigma^y_{zx} = -\sigma^x_{zy}$, and $\sigma^x_{yz} = -\sigma^y_{xz}$, the calculated values of which are listed in Table II. We find that the largest component of the conductivity tensor is σ^x_{zy} (≈ 302 $\frac{\hbar}{e}\Omega^{-1}$cm^{-1}), which corresponds to a spin current along $\hat{z}$ with spin polarization along $\hat{x}$, when the electric field is applied along $\hat{y}$. The SHC is also found to be very anisotropic, which is the result of the anisotropic hexagonal crystal structure. Furthermore, BTIO is expected to have a much larger efficiency for spin current detection than the pure metals such as Pt, due to a much larger spin Hall angle Θ_{SH}, the ratio of the SHC to the charge conductivity, which is the typical figure of merit for spin current detection. The magnitude of the computed SHC in BTIO is comparable to the reported SHC of IrO_2 (≈ 250 $\frac{\hbar}{e}\Omega^{-1}$cm^{-1}) [24]), a material that is commonly used for spin current detection.

Another interesting point is the conversion of the DNL (present along $A \to L$) into a pair of WNLs by breaking the TR symmetry, which can be achieved either by applying an external magnetic field or by doping with magnetic ions. This would provide a mechanism for creating WNLs, with the potential to host exotic surface states. For the existence of the WNLs [25], we must have either the TR or the inversion symmetry, but not both. It is easy to see from the wave function symmetry in Table I and our earlier arguments that with the broken TR symmetry, the four-fold degeneracy along $A \to L$ breaks into a pair of doubly-degenerate WNLs. We illustrate this by computing the band structure by adding in the TB Hamiltonian Eq. (2) an extra magnetic field term along the $\hat{z}$ direction, $\mathcal{H}_{\mathrm{mag}} = -B\sum_{i\mu}\sum_{\sigma,\sigma'} c^{\dagger}_{i\mu\sigma}\sigma^z_{\sigma\sigma'}c_{i\mu\sigma'}$. The results are shown in Figs. 3 (d) and (e), with the latter showing the two-fold degenerate WNLs along $A \to L$.

In conclusion, we have predicted the presence of DNL in BTIO, a known compound that has been synthesized some time ago. A number of Dirac nodal lines and loops exist in the absence of the SOC, while with the introduction of SOC, only a star-like DNL along $A \to L$ is protected by the non-symmorphic glide reflection. The remaining DNLs, not protected by symmetry, gap out in the presence of the SOC, leading to a large SHC. The expected large efficiency for spin current detection (spin Hall angle Θ_{SH}) indicates the potential application of BTIO as a spin current detector. The DNLs can easily be probed by angle-resolved photoemission spectroscopy, which can reveal the band crossings predicted for this material. Further materials containing DNLs are expected to show unusual electronic properties as compared to materials hosting nodal points or the conventional metals [24, 26]. In fact, the DNLs in IrO_2 have been proposed to be responsible for the observed large magnetoresistance in this material [24]. In view of this, it would be interesting to investigate the transport properties of BTIO experimentally. Finally, as our symmetry results are not restricted to the present compound only, it would be useful to look for the entire family of materials belonging to the same space group [27] as potential candidates to host DNL, and possibly with large SHC as well.

We thank the U.S. Department of Energy, Office of Basic Energy Sciences, Division of Materials Sciences and Engineering for financial support under Grant No. DEFG02-00ER45818.

[1] X. Wan, A. M. Turner, A. Vishwanath, and S. Y. Savrasov, Topological semimetal and Fermi-arc surface states in the electronic structure of pyrochlore iridates, Phys. Rev. B **83**, 205101 (2011).

[2] G. Bian *et. al*, Topological nodal-line fermions in spin-orbit metal $PbTaSe_2$, Nat. Commun. **7**, 10556 (2016).

[3] W. C. Yu, X. Zhou, F.-C. Chuang, S. A. Yang, H. Lin, and A. Bansil, Nonsymmorphic cubic Dirac point and crossed nodal rings across the ferroelectric phase transition in $LiOsO_3$, Phys. Rev. Mater. 2, 051201(R) (2018)

[4] S. Jia, S.-Y. Xu, and M. Z. Hasan, Weyl semimetals, Fermi arcs and chiral anomalies, Nat. Mater. **15**, 1140-1144 (2016).

[5] W. B. Rui, Y. X. Zhao, and A. P. Schnyder, Topological transport in Dirac nodal-line semimetals, Phys. Rev. B **97**, 161113(R) (2018).

[6] S. T. Ramamurthy, and T. L. Hughes, Quasitopological electromagnetic response of line-node semimetals, Phys. Rev. B **95**, 075138 (2017).

[7] A. A. Burkov, M. D. Hook, and L. Balents, Topological nodal semimetals, Phys. Rev. B **84**, 235126 (2011).

[8] Z. Wang, A. Alexandradinata, R. J. Cava, and B. A. Bernevig, Hourglass fermions, Nature (London) **532**, 189 (2016).

[9] K. Shiozaki, M. Sato, and K. Gomi, Z2 topology in nonsymmorphic crystalline insulators: Möbius twist in surface states, Phys. Rev. B **91**, 155120 (2015).

[10] T. Bzdušek, Q. S. Wu, A. Regg, M. Sigrist, and A. A. Soluyanov, Nodal-chain metals, Nature (London) **538**, 75 (2016).

[11] R. Yu, Q. Wu, Z. Fang, and H. Weng, From Nodal Chain Semimetal to Weyl Semimetal in HfC, Phys. Rev. Lett. **119**, 036401 (2017).

[12] B. Singh, B. Ghosh, C. Su, H. Lin, A. Agarwal, and A. Bansil, Topological Hourglass Dirac Semimetal in the Nonpolar Phase of Ag_2BiO_3, Phys. Rev. Lett. **121**, 226401 (2018).

[13] M. I. Dyakonov, and V. I. Perel, Possibility of Orienting Electron Spins with Current, Sov. Phys. JETP Lett. **13**, 467 (1971); J. E. Hirsch, Spin Hall Effect, Phys. Rev. Lett. **83**, 1834-1837 (1999).

[14] S. K. Panda, S. Bhowal, Y. Li, S. Ganguly, R. Valentí, L. Nordström, and I. Dasgupta, Electronic structure and spin-orbit driven magnetism in $d^{4.5}$ insulator $Ba_3YIr_2O_9$, Phys. Rev. B **92**, 180403(R) (2015); A. Nag *et. al*, Origin of the Spin-Orbital Liquid State in a Nearly J = 0 Iridate $Ba_3ZnIr_2O_9$, Phys. Rev. Lett. **116**, 097205 (2016).

[15] T. Sakamoto, Y. Doi , Y. Hinatsu, Crystal structures and magnetic properties of 6H-perovskite-type oxides $Ba_3MIr_2O_9$ (M = Mg, Ca, Sc, Ti, Zn, Sr, Zr, Cd and In), J. Solid State Chem. **179**, 2595-2601 (2006).

[16] S. Bhowal, S. Ganguly, and I. Dasgupta, Spin-orbit coupling driven novel magnetism in d^5 6H-perovskite iridates $Ba_3IrTi_2O_9$ and $Ba_3TiIr_2O_9$, J. Phys. Condens. Matter **31**, 185802 (2019).

[17] J. P. Perdew, K. Burke, and M. Ernzerhof, Generalized Gradient Approximation Made Simple, Phys. Rev. Lett. **77**, 3865 (1996).

[18] G. Kresse and J. Furthmüller, Efficient iterative schemes for *ab initio* total-energy calculations using a plane-wave basis set, Phys. Rev. B **54**, 11169 (1996).

[19] C. Bradley and A. P. Cracknell, The Mathematical Theory of Symmetry in Solids: Representation theory for point groups and space groups (Clarendon Press, Oxford, 1972); L. Elcoro, B. Bradlyn, Z. Wang, M. G. Vergniory, J. Cano, C. Felser, B. A. Bernevig, D. Orobengoa, G. de la Flora, and M. I. Aroyo, Double crystallographic groups and their representations on the Bilbao Crystallographic Server, J. Appl. Cryst. **50**, 1457-1477 (2017).

[20] O. K. Andersen and T. Saha-Dasgupta, Muffin-tin orbitals of arbitrary order, Phys. Rev. B **62**, R16219 (2000).

[21] See Supplemental Materials describing breakdown of contributions to the spin Hall conductivity from various parts of the Brillouin zone and total density of states, which include Ref. [22]

[22] V. T. N. Huyen, M.-T. Suzuki, K. Yamauchi, and T. Oguchi, Topology analysis for anomalous Hall effect in the non-collinear antiferromagnetic states of Mn_3AN (A = Ni, Cu, Zn, Ga, Ge, Pd, In, Sn, Ir, Pt), arXiv:1905.07962 (2019); W. S. Choi, S. S. A. Seo, K. W. Kim, and T. W. Noh, Dielectric constants of Ir, Ru, Pt, and IrO_2: Contributions from bound charges, Phys. Rev. B **74**, 205117 (2006).

[23] M. Seemann, D. Ködderitzsch, S. Wimmer, and H. Ebert, Symmetry-imposed shape of linear response tensors, Phys. Rev. B **92**, 155138 (2015).

[24] Y. Sun, Y. Zhang, C.-X. Liu, C. Felser, and B. Yan, Dirac nodal lines and induced spin Hall effect in metallic rutile oxides, Phys. Rev. B **95**, 235104 (2017).

[25] S.-Y. Yang, H. Yang, E. Derunova, S. S. P. Parkin, B. Yan, and M. N. Ali, Symmetry demanded topological nodal-line materials, Adv. Phys X **3**, 1414631 (2018).

[26] C. Fang, Y. Chen, H.-Y. Kee, and L. Fu, Topological nodal line semimetals with and without spin-orbital coupling, Phys. Rev. B **92**, 081201(R) (2015); Y. Huh, E.-G. Moon, and Y. B. Kim, Long-range Coulomb interaction in nodal-ring semimetals, Phys. Rev. B **93**, 035138 (2016).

[27] Y. Yanase and K. Shiozaki, Möbius topological superconductivity in UPt_3, Phys. Rev. B **95**, 224514 (2017).